

# Author response to the revised manuscript version

This document repeats the questions of all referees with the corresponding authors' responses on a point to point basis. Additionally, it indicates for every comment the changes made in manuscript and explains the reasoning of the authors if needed. All page and line references refer to the revised manuscript version. Appended to this document is a differential view between the first and revised manuscript version for convenient tracking of the applied changes.

## 1 General comments Referee 1

R1: *This is a well written paper. However, what this paper is currently missing in my opinion is visualization of the measured and processed data. Can you please add visualizations of actual measured data (both spectral and images) and results from each of the modeling steps? It would be interesting for readers to see how speckle patterns of that diffuser look and the pattern propagation to the final imaging plane. Can you also add some figures from the laser spectra used? Just as background information you could include in the introduction that sources like lasers produce temporal speckle and diffusers produce spatial speckle. Speckle pattern created by a diffuser can be averaged for example by rotating the diffuser during the measurement.*

Response: We will add figures illustrating the speckle patterns in the slit and detector plane. The width of the laser line is presented in Section 3. We will also add more detailed explanations and motivations regarding speckle effects and some mitigation principles.

Changes in manuscript: We added Figure 2, which shows the measurement data at the intermediate steps in the measurement chain. The width of the laser line is given in lines 138 and 148 according to supplier specifications. We introduced into the subject of speckle and some reduction aspects in the introduction (lines 20-34).

R1: *This is slightly off from the focus on algorithm development itself, but very important what comes to the proper operation of the instrument. What are the criteria for the diffuser to reduce speckle effect and how does that affect overall performance of the instrument? Are there any tradeoffs?*

Response: Generally, the SFA will be lower the more independent speckle patterns per wavelength band a diffuser generates. For example, the NIR instrument used in this work would generate about 56 independent patterns ( $M_{spectral}$ ) over a spectral range equal to the resolution  $\lambda_{res}$  at 776nm. This number is influenced by the sensitivity of the diffuser with respect to wavelength change. This sensitivity is significantly higher for transmission geometries, since it will yield a wider range of possible optical path differences. This effect also scales with the thickness of the diffuser. As far as our experience goes: a thicker diffuser also means less transmission and therefore less signal on the detector during calibration.

Changes in manuscript: No specific changes were made.

R1: *Maybe you could add reasoning why this specific glass volume diffuser was selected and refer to studies on some diffuser contamination and radiation tests? Contamination/degradation of the diffusers is to my understanding a major issue in satellite measurements. This is at least a problem at UV and visible and it has much larger effect than speckle. Since diffraction limit increases at longer wavelengths, at NIR and SWIR diffuser speckle is worse than at visible spectral range. You could mention this in the paper.*

Response: The specific diffuser material was chosen for the measurements since it was qualified for the Sentinel 5/UVNS (see Irizar et al. (2019)). We will mention this when describing the material in section 3.2. The impact of speckles generated by longer wavelengths can be seen in the smaller averaging factor  $M_{spectral}$  of the SWIR band compared to the NIR. We will point this out during the discussion of the results.

Changes in manuscript: A justification for the diffuser material is now given in lines 132-134. An interpretation to the spectral averaging factor  $M_{spectral}$  is given in lines 262/263 and Figure 5 shows the SFA scaling with wavelength explicitly.

## 2 Specific comments Referee 1

**Page 1, row 22:** R1: *“... spectrometers with fine spectral resolution and strict demands to radiometric accuracy...” You could specify these “strict demands” in the paper. At least stray light is usually a problem in imaging spectrometers.*

Response: We will clarify that diffuser speckles need to be considered as part of the radiometric accuracy error budget next to other contributors such as stray-light or polarization.

Changes in manuscript: Lines 24-26.

**Page 1, row 29:** R1: *“...end-to-end measurements by van Brug and Courrèges-Lacoste (2007) as well as models for different speckle averaging effects...” Can you explain in detail what end-to-end measurements were these and what existing speckle averaging methods are available (both hardware and software)?*

Response: We will add an explanation regarding the end-to-end measurements. The authors are convinced, that the effects of diffuser speckle can not be reliably characterized with representative end-to-end setups (which includes a full spectrometer, telescope optics, diffuser and light source). The suppression of the speckle effects is implicit to the design of the instrument. Therefore, if one

were to measure speckle residuals with a certain setup, it can not be representative for an instrument that is supposed to have a neglectable residual speckle amplitude (SFA).

Changes in manuscript: Detailed explanation regarding those aspects can be found in lines 20-34 and 38-44.

**Page 5, Figure 2:** R1: *Regarding the setup, please specify the type of optical fibers used between the tunable laser source and the fiber tab and between the fiber tab and the fiber output. You could say that since your spectral tuning range is narrow, you can use single mode fibers to transmit the laser beam and create uniform illumination. You could also show in a figure how spatially uniform the radiation output from the single mode fiber is before it hits the diffuser. Is there any spatial speckle created by the single mode fiber? You could mention that multimode fibers should not be used as they generate severe spatial speckle that can be worse than the diffuser speckle. The speckle pattern by the multimode fiber changes when the fiber bends only slightly. In addition, can you please draw Figure 2 so that it is easier to see which cables are optical fibers and which of them are electrical cables.*

Response: We will specify the exact fiber types used, include the result of spatial beam uniformity measurements at the diffuser plane, and add the referee's suggested comments regarding multi mode fibers. We will also correct Figure 2. The spatial uniformity measurements showed no apparent spatial speckles generated by the fibers, which we will mention as well.

Changes in manuscript: Information about the used fibers were added in lines 127-129, 138/139, and 147. Spatial uniformity is given in lines 135-137. Figure 2 is now Figure 3 and is corrected.

**Page 5, Figure 2:** R1: *Please replace "Powermeter" with "Power meter".*

Response: Done.

Changes in manuscript: see Figure 3.

**Page 5, rows 109-111:** R1: *Can you please give references to these data products?*

Response: Done.

Changes in manuscript: see lines 124-125.

**Page 5, row 110:** R1: *Please replace "... CO2, Aerosols, or the O2 absorption..." with "... CO<sub>2</sub>, aerosols, or the O<sub>2</sub> absorption ..."*

Response: Done.

Changes in manuscript: line 123.

**Page 6, rows 117-118:** R1: *“For the NIR the laser source has a center wavelength of 780 nm and a nominal linewidth of 300 kHz.” Can you give the nominal linewidth in wavelengths?*

Response: Done.

Changes in manuscript: see line 138.

**Page 6, rows 125-126:** R1: *“The SWIR laser source center wavelength is 1550 nm, with single mode output of nominal 150 kHz linewidth.” Can you give the nominal linewidth in wavelengths?*

Response: Done.

Changes in manuscript: see line 148.

**Page 6, row 129:** R1: *Please define a speckle oversampling ratio*

Response: We will provide an explanation without this confusing term. It states how many detector pixel the speckle correlation areas are being sampled with.

Changes in manuscript: The sampling of speckle in the slit plane are explained in lines 143 and 151.

**Page 6, row 162:** R1: *Please define  $f_m$ .*

Response: We will change this part slightly to be more understandable, also introducing the symbol  $\Delta f$  correctly.

Changes in manuscript: We now use symbols with wavelength dependency instead of frequency, because the description is easier to understand in our opinion.

**Page 7, row 167:** R1: *You have an error in the spatial offset equation.... How does correcting this affect the results?*

Response: The symbol " $\Delta f$ " was used incorrect at some instances, which led to the misleading expression for  $\Delta b$ . It will be corrected accordingly.

Changes in manuscript: We now give symbols with wavelength dependency instead of frequency, which simplifies this expression.

**Page 8, row 172:** R1: *Please present exact equation for the path length probability density function  $p(l)$ .*

Response: We will use a direct analytic expression for  $F(\Delta f)$  given by Zhu et al. (1991), which lead to similar results. However, this way one does not need to detour of calculating  $p(l)$  first and taking the Fourier transform after. Also this expression gives direct access to the angular correlation function, too, which is interesting for estimations of angular contributions in the future. For the interested reader see Patterson et al. (1989), where an expression for  $p(l)$  is derived explicitly.

Changes in manuscript: see Equation (10) and following lines.

**Page 8, row 178:** R1: *There is one extra parenthesis, please replace  $\Delta b(\Delta f)$  with  $\Delta b(\Delta f)$ .*

Response: We will use the symbol " $\Delta b$ " without the explicit frequency dependence.

Changes in manuscript:  $\Delta b$  is now defined in line 194.

**Page 8, row 180:** R1: *There is a typing error in Equation (10), the integrals' limits should be  $\int_{-\infty}^{\infty}$  instead of  $\int_{\infty}^{\infty}$ .*

Response: Done.

Changes in manuscript: see Equation (11).

**Page 8, row 181:** R1: *"... $P(h)$  is the aperture function of the imaging system ...". Please present the exact equation for  $P(h)$ .*

Response: We will give an example for a circular aperture now.

Changes in manuscript: see line 212.

**Page 10, row 225:** R1: *"Therefore, the resultant speckle correlation function at the detector  $\mu_{det}(\Delta a, \Delta b)$  is a convolution of ...". Please present  $\mu_{det}(\Delta a, \Delta b)$  as an equation.*

Response: We will present an equation.

Changes in manuscript: see Equation 20.

**Page 10, row 250:** R1: *"We assume, that detector noise is averaged in this step" Can you please add what the noise properties of the detector are (e.g. in  $V/\sqrt{Hz}$ ) and what integration times were used?*

Response: We will present a complete rework regarding the uncertainties for the averaging factors and the SFA.

Changes in manuscript: First, a discussion of detector noise is given in line 278-279 suggesting why speckles are not measured with contrast of unity, which also happened in other studies. However, this contribution is constant and does not change the measurement result, because we compensate it by comparing contrast levels and then assume an initial contrast of unity. Secondly, any detector noise is indirectly accounted for in the estimation of uncertainties for the averaging factors discussed in lines 286-297. We basically characterized fluctuations in the two functions  $F$  and  $\Psi$ , that basically govern both averaging factors. Additionally, a more significant factor for  $M_{detector}$  seems to be a statistical effect regarding the standard deviation estimator. A direct approach is tedious in our opinion, since noise should vary significantly over a single speckle image.

**Page 10, Subsection 4.4 Predicted SFA:** R1: *Since this subsection includes only one sentence, to me it makes more sense to remove this subsection 4.4 and move the equation to the beginning of Section 4, right after Eq. (7). There you could also define  $M_{polarization}$ ,  $M_{spectral}$ , and  $M_{detector}$  and link these symbols to the steps 1, 2, and 3.*

Response: Done.

Changes in manuscript: see lines 173-178.

**Page 11, Table 2:** R1: *Based on the values of  $M_{polarization}$ ,  $M_{spectral}$ , and  $M_{detector}$ , the SFA on the first row of Table 2 should be 0.0039 (not 0.0040). Can you please give SFAs in percents in Table 2?*

Response: We will include an error analysis and also fixed a minor inconsistency in our spectrometer propagation, which caused some systematic deviations in the measured averaging factors, especially for the NIR band.

Changes in manuscript: SFA values is given in percent now in Table 2. For the derivation of uncertainties see lines 286-297. We fixed a numerical (rounding) problem in our spectrometer propagation. This involved slightly changing the spectral resolution of the instrument in the NIR. We also had to shorten the tuning range because of some systematic environmental influences. For the SWIR band we slightly increased the step size  $\Delta\lambda$  from 2.5 pm to 3.1 pm (see Table 1) and were able to increase the tuning range in an attempt to decrease the uncertainty for  $M_{detector}$  (which depends on number of spectral pixel rows, hence the tuning range). Also we increased the apertures' diameter from 10 mm to 13 mm to increase SNR.

**Page 11, row 254:** R1: *"It is also dependent on detector noise, which explains slightly higher averaging factors than predicted." Can you predict noise proper-*

*ties of the detector used and add them to the calculations?*

Response: We will rework the discussion of uncertainties.

Changes in manuscript: see changes of the comment above.

**Results section:** R1: *How much diffuser speckle contributes to the overall measurement uncertainty?*

Response: The relative spectral radiometric accuracy (RSRA) budget of ESA's CO2M mission is 0.5% for all bands (see Meijer et al.). However, the SFA results presented in this work should not be directly compared to this budget, since it does not account for angular averaging effects. The SFA including those effects can be two orders of magnitude lower.

Changes in manuscript: Since we did not present a detailed analysis of angular averaging mechanisms in this study a absolute comparison to a realistic error budgets seems inappropriate at this point. However, we do explain in the conclusion how the results in this work fit into a complete description of all averaging effects in an imaging spectrometer that are present to our knowledge.

### 3 General comments Referee 2

R2: *The developed model is physically sound and has been validated using laboratory measurements at two wavelengths. While the technical content is complete and well explained, I miss some motivation and explanation of the effect in the Introduction and an illustration and discussion of the practical relevance in the Results and Discussion section. I recommend publication after these minor revisions are made.*

Response: We will add more detailed explanations and motivations regarding speckle effect into the introduction and extend the discussion in order to better illustrate our results.

Changes in manuscript: We added a more comprehensive introductory part in lines 20-44. We give an interpretation of the determined averaging factor in lines 262-264 and the scaling with wavelength in Figure 5 and lines 296-299.

### 4 Specific comments Referee 2

R2: *The modeled effect is not well known in the scientific community. It is difficult to believe that sunlight induces noticeable interference effect in solids because speckles are typical for lasers, but not for natural light. You should mention in the Introduction the puzzling spectral wiggles in the order of a few percent discovered in data of the SCIAMACHY and OMI instruments (described and illustrated by van Brug et al., 2004).*

Response: We will clarify these aspects in the introduction.

Changes in manuscript: see lines 20f.

R2: *Interference effects require that the coherence length is larger than the size of material inhomogeneities, thus you should quantify the coherence length of sunlight and compare it with the typical scale of inhomogeneities in diffuser material. According to Divitt and Novotny (2015) the coherence length of sunlight is 80 x wavelength, which corresponds to 62  $\mu\text{m}$  and 126  $\mu\text{m}$  at the wavelengths of your measurements (777 nm, 1570 nm).*

Response: According to the specifications given by the manufacturer the scattering centers of the diffuser material have a maximum diameter of 20 microns. We will add a comparison in Section 3.2.

Changes in manuscript: see lines 130-134.

R2: *The importance of the effect and the model for practical applications should*

be graphically illustrated in the Results and Discussion sections. In particular a plot of the wavelength dependency should be added due to its high relevance for spectral measurements. The wavelength dependency cannot be assessed from the equations, thus a graphical illustration would help the reader to grasp the importance of the described effect. Furthermore, such a plot would allow comparing at least qualitatively the modelled spectral dependency with observed spectral patterns, e.g. as in Fig. 1 of van Brug et al. (2004).

Response: We will add plots of the wavelength dependence for both bands in the discussion.

Changes in manuscript: see Figure 5 and lines 296-299 as well as Figure 4.

R2: *You should also mention that the effect is not restricted to diffusers, but occurs for all static measurements of a solid. Point out its relevance for laboratory calibration of spectrometers and spectral measurements using a fixed set-up of target, spectrometer and light source; and explain that the effect vanishes if one of these is moved or tilted during the measurement, as in case of remote sensing.*

Response: We will introduce the reader more broadly into the subject of speckle and some mitigation methods in the introduction. However, we would like to point out, that the movement or the tilting of parts in the optical system are usually not implemented in space applications, since they would involve additional moving parts, which is usually to be avoided. The only change of the geometry would be the angle of incident due to the movement of the instrument relativ to the sun. Angular averaging effects, however, are not part of this work.

Changes in manuscript: See lines 20-34.

**Line 21f:** R2: *"Since Spectral Features are of statistical nature and cannot be mitigated by any post-processing steps". Correction may indeed be difficult, but not because the effect is of statistical nature, but because the intensity of the pattern and its position on the focal plane are difficult to calculate accurately because they depend on a number of parameters which are difficult to measure with sufficient accuracy (temperature, pressure, isotropy of incident light field).*

Response: We will adapt this passage regarding the term "statistical".

Changes in manuscript: We removed the term statistical (line 18) and build the argumentation beginning in line 20 to line 32 regarding the quasi statistical treatment of the speckle effect.

## 5 Technical corrections Referee 2

**Line 18:** R2: : *"diffuser introduces a statistical interference phenomenon" I suggest to delete statistical (as it is a geometric effect, not a statistical one) and replace "phenomenon" by "pattern".*

Response: We see the argument of the Referee here and will follow his suggestion to remove "statistical" for this specific formulation. However, we still see the need for a quasi statistical treatment of the effect, because the resulting intensity of the speckle pattern seen by the detector is essentially unpredictable.

Changes in manuscript: see line 18 and lines 20-32.

**Line 50:** R2: : *unwanted "features". Unclear: What do you mean with unwanted? Unexplained?.*

Response: What is meant here, are the "features", that are caused solely by the diffuser. They are "unwanted" in the sense, that they alter the solar reference spectrum, which is recorded during calibration. We will change this sentence to clarify this.

Changes in manuscript: see lines 61f.

**Line 51f:** R2: : *The SFA value is then calculated as the standard deviation of the normalized signal over a certain spectral width, that includes multiple features." The definition of SFA is unclear: normalized to what? What means "certain spectral width"? Is standard deviation calculated over time or over wavelength? The definition only gets clear at line 106f together with Eq. (3). Improve here the explanation and refer for details to Eq. (3).*

Response: We will replace "certain wavelength range" by "multiple spectral channels". The standard deviation is taken over the normalized detector signal, which essentially is calculating it over wavelength. We will clarify this.

Changes in manuscript: see lines 62f. We refer to Section 3.2 for details.

**Line 76f:** R2: : *"Sun's light... is assumed to be spatially coherent giving the distance from the Sun to the Earth and the limited acceptance angle of the spectrometer." The coherence of light from a spatially incoherent spherical source is in fact valid immediately beyond a distance of a few wavelengths (Agarwal et al. 2004), thus the spatial coherence of sunlight has nothing to do with the Earth-sun distance. Quantify instead the coherence length, e.g. by citing the result  $80 * \lambda$  by Divitt and Novotny (2015). Also the influence of the acceptance angle of the spectrometer is not clear. Either explain or remove it.*

Response: We wanted to point out that the spatially coherent Sun light incident on the diffuser can be treated as collimated under the mentioned conditions, which is also matched by our experimental setup. We will rework this part.

Changes in manuscript: see lines 88-89.

**Line 77f:** R2: : *"the temporal coherence is very short compared to the detector integration time, which is in the order of seconds" Quantify the temporal coherence and replace seconds by milli-seconds. The sunlight coherence time is 3 fs according to Herman et al. (2014) who cite the "Optics" book of Hecht (2016).*

Response: We will rework this part.

Changes in manuscript: see lines 87-92.

**Line 120:** R2: : *add a reference for Eq. (4).*

Response: Done.

Changes in manuscript: see line 143.

**Line 233f:** R2: : *"the fitted mean free path length of our diffuser sample is determined as  $l_s = 53\mu\text{m}$ ". Explain how you fitted the free path length. The mean free path length depends on wavelength as the scattering probability is wavelength-dependent. Hence, add the wavelength.*

Response: We will use different values for  $l_s$  for each band. We will add an explanation on how this values were obtained. The reference value of  $l_s = 56\mu\text{m}$  given by the manufacturer is for  $\lambda = 500\text{nm}$ . We obtained more realistic values for  $l_s$  at the employed wavelengths using the approach by Zhu et al. (1991) of calculating the frequency correlation function  $F(\Delta f)$ .

Changes in manuscript: see Equation (10) and following lines, Table 1, Figure 4, and lines 265-270. Note that we used the wavelength dependence for  $F$  and that we changed  $l_s$  to  $l_t$ , which denotes the transport mean free path. This is more appropriate for anisotropic multi scattering systems.

**Line 300:** R2: : *Coernicus  $\rightarrow$  Copernicus.*

Response: Done.

Changes in manuscript: see line 362.

## 6 References

- Zhu, J. X., Pine, D. J., and Weitz, D. A.: Internal reflection of diffusive light in random media, *Phys. Rev. A*, 44, 3948–3959, <https://doi.org/10.1103/PhysRevA.44.3948>, <https://link.aps.org/doi/10.1103/PhysRevA.44.3948>, 1991.
- Patterson, M. S., Chance, B., and Wilson, B. C.: Time resolved reflectance and transmittance for the noninvasive measurement of tissue optical properties, *Appl. Opt.*, 28, 2331–2336, <https://doi.org/10.1364/AO.28.002331>, <http://ao.osa.org/abstract.cfm?URI=a28-12-2331>, 1989.
- Irizar, J., Melf, M., Bartsch, P., Koehler, J., Weiss, S., Greinacher, R., Erdmann, M., Kirschner, V., Albinana, A. P., and Martin, D.: Sentinel-5/UVNS, in: International Conference on Space Optics 2018, edited by Sodnik, Z., Karafolas, N., and Cugny, B., vol. 11180, pp. 41 – 58, 315 International Society for Optics and Photonics, SPIE, <https://doi.org/10.1117/12.2535923>, <https://doi.org/10.1117/12.2535923>, 2019.
- Meijer, Y., Boesch, H., Bombelli, A., Brunner, D., Buchwitz, M., Ciais, P., Crisp, D., Engelen, R., Holmlund, K., Houweling, S., Janssens- Meanhout, G., Marshall, J., Nakajima, M., B.Pinty, Scholze, M., Bezy, J.-L., Drinkwater, M., Fehr, T., Fernandez, V., Loescher, A., Nett, H., and Sierk, B.: Coernicus CO2 Monitoring Mission Requirements Document, techreport 2, European Space Agency, Earth and Mission Science Division, 2019.

# Prediction Model for Diffuser Induced Spectral Features in Imaging Spectrometers

Florian Richter<sup>1,2</sup>, Corneli Keim<sup>2</sup>, Jérôme Caron\*, Jasper Krauser<sup>2</sup>, Dennis Weise<sup>2</sup>, and Mark Wenig<sup>1</sup>

<sup>1</sup>Meteorological Institute LMU Munich, Theresienstr. 37, Munich, Germany

<sup>2</sup>Airbus Defence and Space GmbH, Willy-Messerschmitt-Str. 1, 82024 Taufkirchen, Germany

\* now at TNO, Optics Department, Stieltjesweg 1, 2628 CK Delft, The Netherlands

**Correspondence:** Florian Richter (flo.richter@physik.lmu.de)

**Abstract.** Wide-field spectrometers for Earth Observation missions require inflight radiometric calibration, for which the Sun can be used as a known reference. Therefor a diffuser is placed in front of the spectrometer in order to scatter the incoming light into the entrance slit and provide homogeneous illumination. The diffuser however, introduces interference patterns known as speckles into the system, yielding potentially significant intensity variations at the detector plane, called Spectral Features.

5 There have been several approaches implemented to characterize the Spectral Features of a spectrometer, e.g. end-to-end measurements with representative instruments. Additionally, in previous publications a measurement technique was proposed, which is based on the acquisition of monochromatic speckles in the entrance slit following a numerical propagation through the disperser to the detection plane. Based on this measurement technique we present a standalone prediction model for the magnitude of Spectral Features in imaging spectrometers, requiring only few input parameters and therefor mitigating the need  
10 for expensive measurement campaigns.

## 1 Introduction

Many current and future Earth Observation missions carry wide field spectrometer payloads such as the ENVISAT Medium Resolution Imaging Spectrometer (Olij et al. (1997)), the Sentinel-2 MultiSpectral Imager (Martimort et al. (2012)), the Sentinel-3a Ocean and Land Colour Imager (Nieke and Mavrocordatos (2017)), the Sentinel-4 UVN instrument (Clermont  
15 et al. (2019)), the Sentinel-5-UVNS instrument (Guehne et al. (2017)), or the GHGIS instrument of CO2M or former Carbon-Sat (Fletcher et al. (2015)). These ~~space~~-~~space~~ based instruments require inflight radiometric calibration, for which the Sun can be used as a known reference. In order to ensure homogeneous illumination of the instrument a diffuser is used to scatter the incoming sunlight into the entrance slit. However, the diffuser introduces a ~~statistical interference phenomenon~~-~~interference~~  
20 ~~pattern~~ known as speckles into the optical system. The speckles propagate through the disperser and are integrated at the detector plane, yielding intensity variations described as *Spectral Features* by van Brug et al. (2004). ~~Since Spectral Features are of statistical nature and cannot be mitigated by any~~-~~When the solar spectrum is used for the calibration of the top of atmosphere measured spectra, the Spectral Features create a radiometric error as they alter the calibration function. Speckle effects are commonly known from applications involving highly coherent laser light such as holographic imaging (Bianco et al. (2018)) or Laser Speckle Contrast Imaging (Heeman et al. (2019)). In general, diffuse sunlight does not yield a significant net speckle~~

25 pattern when incident on a detector due to its broad spectrum. However, for spectrometers with a fine spectral resolution, the spectral width per channel is narrow enough to give rise to an amplitude of the Spectral Features, that can be as large as other radiometric errors, e.g. due to straylight and polarisation. Spectral Features depend on various geometric conditions implying that their exact position at the detector plane cannot be reliably predicted. This also renders any mitigating post-processing steps  ~~, they may pose a significant contributor ineffective.~~ Widely known speckle suppression techniques, such as  
30 rotation or tilting of elements in the optical system (Goodman, 2007, section 5), are only viable for on-ground calibration with a static setup. For space applications additional moving parts are typically not implemented, because they pose a supplementary risk of failure. In early planning phases, each contribution to the radiometric error  ~~budget. In particular for spectrometers with fine spectral resolution and strict demands to radiometric accuracy it is important to determine the severity of this error in an instrument even in early planning phases. The magnitude of this error is commonly described in terms~~ needs to  
35 be quantitatively estimated to allow a global optimization of the instrument. This work presents a novel method to predict the radiometric error due to Spectral Features. As in most applications, the radiometric error is driven by the amplitude of the Spectral Features, van Brug and Courrèges-Lacoste (2007) introduced the Spectral Features Amplitude (SFA)  ~~first introduced by van Brug and Courrèges-Lacoste (2007)~~ as a standardized measure.

The issue of diffuser induced Spectral Features in imaging spectrometers has first been documented by Richter et al. (2002) and Wenig et al. (2004) in the context of the Global Ozone Monitoring Experiment (GOME). Ahlers et al. (2004)  
40 observed spectral oscillations caused by the onboard diffuser in the Scanning Imaging Absorption Spectrometer for Atmospheric Cartography (SCIAMACHY) instrument, as well as van Brug et al. (2004). Several approaches for characterization and modeling have been proposed since, ~~e.g.,~~ van Brug and Courrèges-Lacoste (2007) presented an end-to-end ~~measurements by van Brug and Courrèges-Lacoste (2007) as well as~~ measurement setup featuring a complete instrument including source,  
45 telescope optics, disperser, and detector. However, since Spectral Features need to be suppressed "by design" of certain instrument parameters a quantitative analysis with a representative spectrometer is usually difficult to achieve. van Brug and Scalia (2012) introduced ~~models for different speckle averaging effects derived by van Brug and Scalia (2012).~~ However, a comprehensive and reliable model has not been presented, yet. Isolating the Spectral Features by eliminating all other error sources in an representative end-to-end setup remains the main challenge to gain quantitative insights into the SFA dependence.

50 A different approach to quantify Spectral Features was taken by Burns et al. (2017) and improved by Richter et al. (2018). It is based on the subsequent acquisition of monochromatic speckle patterns in the slit plane over ~~a certain wavelength range~~ several spectral channels, which are then propagated numerically through the disperser to the detection plane. Some simplifying assumptions are made about the optical system which reduces the complexity and limits systematic error contributions. It is only limited by the SNR and the resolution achieved in the entrance slit and therefor capable of yielding comprehensive  
55 measurement data ~~. Most important for most instrument designs. Especially,~~ it allows for a step-by-step tracing of the speckle statistics from the slit to the detector plane.

Based on this SFA measurement technique we present a novel standalone SFA prediction model, which solely relies on mathematical descriptions of the speckle statistic and its SFA impact. It includes polarization effects of the diffuser, spatial and spectral averaging as well as pixel averaging at the detector.

60 First we review the definition of the Spectral Features Amplitude (SFA) in Sect. 2. In Sect. 3 the revised SFA measurement technique used for our measurements is shown. We then present the standalone SFA prediction model in Sect. 4, which can be understood as a mathematical formulation of the SFA measurement technique. Finally, we compare the results of the prediction model to our measurement chain in detail in Sect. 5 to show its validity. In the last section we ~~dieuss~~discuss the applicability to a real instrument.

## 65 2 Spectral Features Amplitude

The term *Spectral Features Amplitude* (SFA) was first proposed by van Brug and Courrèges-Lacoste (2007) as ~~generic method~~standardized way to quantify diffuser induced "wiggles" in a spectrum measured by a space spectrometer instrument. They describe it as the magnitude of ~~unwanted the~~ "features" ~~that are left in the spectrum when subtracting all other features like emission lines from the source and atmospheric absorption~~in a spectrum that are solely caused by the diffuser altering the  
70 solar reference spectrum. The SFA value is ~~then~~ calculated as the standard deviation of the ~~normalized signal over a certain spectral width, that includes multiple features.~~mean normalized detector signal over multiple spectral channels (see details in Sect. (3.1)). The SFA value holds information about the amplitude of features. However, the data produced in this work, which is used to calculate the SFA, also allows for the estimation of the spectral extend of features. One usually may not draw conclusions about the absolute spectral positions of features with this approach. We will show that ~~for high performance~~  
75 ~~volume diffuser, such as the one~~the instrument parameters used in this work ~~lead~~ to a spectral speckle extend smaller than the instrument detector pixel, ~~which.~~ This essentially allows for the treatment of the SFA as white noise at the detector level.

## 3 SFA Measurement Chain

In this Sect. the used SFA measurement technique introduced by Burns et al. (2017) is presented in a revised state. The goal of this technique is the reduction of experimental complexity and therefore systematic error contributions during data acquisition.  
80 First, the measurement principle is explained. Second, the used materials and the measurement procedures for the near infrared (NIR) and the short wavelength infrared (SWIR) channel are presented.

### 3.1 Principle

Figure 1 depicts the optical setup of an imaging spectrometer during solar calibration. The incoming sunlight is scattered by the diffuser. The scattering origin lies in the aperture plane with spatial coordinates  $g$  and  $h$  which is perpendicular to the light's  
85 direction of propagation. The angular field distribution at the aperture plane is imaged to the slit plane with coordinates  $x$  and  $y$ . The light is collimated onto a dispersive element (e.g a diffraction grating), which is splitting it into its spectral components. The spatial information in the  $y$  direction of the slit is transformed into spectral information at the detector with coordinate  $b$  by imaging the the diffracted beams of different wavelengths onto a 2D array detector. Beams of the same wavelength (within the spectral resolution) are assigned the same spectral detector coordinate  $b$ . The spatial information in  $x$  direction is retained

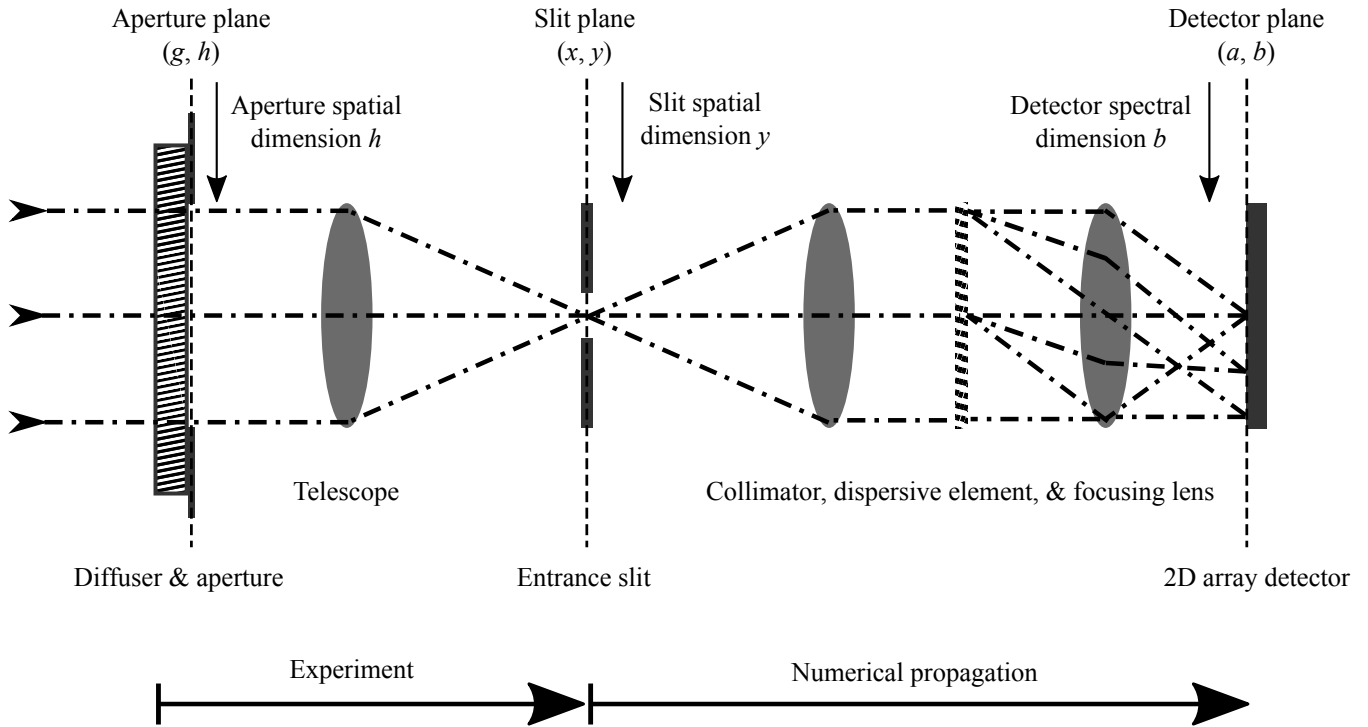


**Figure 1.** Optical setup of an imaging spectrometer during solar calibration. The sequence of optical components is subdivided into two parts. The first part is covered by the experimental setup in the lab starting at the illuminated diffuser and ending at the slit in the telescope focal plane. The second part numerically propagates the images recorded in the slit plane to the instrument focal plane.

90 in the detector coordinate  $a$ . We relate the coordinates via the simplified linear spectrometer equations

$$a = M_x x, \tag{1}$$

$$b = M_y y + k\lambda, \tag{2}$$

where  $M_x$  and  $M_y$  are the respective magnification factors in  $x$  and  $y$  direction,  $k = db/d\lambda$  denotes the dispersion, and  $\lambda$  the wavelength. For these simplified equations to hold the magnification factors and the dispersion are assumed to be independent of the wavelength and the spatial position  $(x, y)$ . Also, the instrument point spread function (IPSF) is not accounted for.

95 ~~Additionally, a few properties of the Sun's light and its detection need to be considered. It is assumed to be spatially coherent giving the distance from the Sun to the Earth and the limited acceptance angle of the spectrometer~~ Sunlight is spatially coherent (Agarwal et al. (2004)) and we can assume collimated light illuminating the diffuser. Additionally, the sunlight's temporal coherence is ~~very short compared to the~~ on the order of femtoseconds (Hecht and Lippert (2018)) and much smaller than the

100 typical detector integration time ~~, which is in the order of seconds. It follows that of several hundred milliseconds of an optical instrument. As a consequence,~~ cross coherence terms of interfering fields of different wavelengths ~~vanish average out~~ and the net intensity distributions at the slit and the detector planes are well approximated by the superposition of monochromatic

intensities. The Sun disk comprises of many incoherent point sources, which should be considered for angular averaging contributions and is not part of this work, as it will only account for a single point source. For the purpose of the SFA measurement the sequence of optical components is subdivided into two parts. The first part ranging from the illuminated diffuser through the telescope to the entrance slit is represented by the optical setup in the lab. The second part comprises the rest of the optical system from the slit plane to the instrument detector plane. The data acquired in the first part is used as input for a numerical simulation of the optical setup after the slit plane. The setup layout is shown in Fig. 3. The Sun is mimicked as a single field point with a tunable laser source, which is spectrally stabilized by a wavemeter, and illuminates the diffuser through a linear polarizer at normal incident with respect to the diffuser plane. The distance between the single mode fiber output and the diffuser is chosen such that the divergent beam illuminates the diffuser homogeneously over the size of the apertures. The second aperture blocks any unwanted angular contributions. A powermeter placed next to the diffuser records a fixed fraction of the emitted laser power. The telescope images the scattered light onto a 2D array detector positioned in the focal plane. The focal plane of the telescope represents the slit plane in Fig. 1. The diffuser plane is tilted by  $10^\circ$  with respect to aperture and slit plane. This ensures that only scattered light contributes to the measurement. The telescope is aligned perpendicular to the aperture and slit plane.

For a measurement, monochromatic speckle intensities are recorded subsequently over a wavelength range  $\lambda_1 \dots \lambda_N$  several times the spectral resolution  $\lambda_{res}$  of the real spectrometer that is being mimicked. [An example for such a monochromatic speckle pattern is shown in Figure 2 \(a\) and \(d\) in the slit plane.](#) The spectral tuning step size  $\Delta\lambda$  in between images needs to be sufficiently small, in order to properly sample the change of the speckle patterns. The intermediate result is a three dimensional data set  $I_{slit}(x, y, \lambda)$  consisting of a spectrum of monochromatic speckle images, where  $x$  and  $y$  are the spatial coordinates in the slit plane and  $\lambda$  is the wavelength. Every speckle image is mapped to a certain position  $(a, b)$  at the focal plane, where all images are summed up in intensity. The summation on intensity basis is justified as cross coherence terms involving interference of different wavelengths of actual sunlight will vanish for sufficiently long integration times. The summation procedure is detailed in Burns et al. (2017) and can be summarized as

$$I_{det}(a, b) = \frac{\Delta\lambda}{\lambda_{res}} \sum_{\lambda=\lambda_1}^{\lambda_N} I_{slit}\left(\frac{a}{M_x}, \frac{b-k\lambda}{M_y}, \lambda\right) \Theta(b-k\lambda), \quad (3)$$

where slit coordinates are expressed in terms of the detector coordinates using Eq. (1) and (2) and the Heavyside function with  $\Theta(y) = 0, y < 0$  and  $\Theta(y) = 1, y \geq 0$ . The result of the sum is a two dimensional intensity distribution in the focal plane of the instrument  $I_{det}(a, b)$ , [which is depicted in Figure 2 \(b\) and \(e\).](#) In a last step  $I_{det}(a, b)$  is overlaid with the actual instruments detector pixel grid  $(\tilde{a}, \tilde{b})$  and intensities belonging to the same pixel are summed, [which is shown in Figure 2 \(c\) and \(f\).](#) The SFA is calculated as standard deviation of the [mean](#) normalized detector pixel intensity distribution  $I_{det, binned}(\tilde{a}, \tilde{b})$ .

### 3.2 Materials and Procedure

Measurements are conducted in the NIR regime around 777 nm and in the SWIR regime around 1570 nm which represent wavelength bands with commonly monitored data products, such as water vapour, clouds, ~~CO<sub>2</sub>, Aerosols~~ CO<sub>2</sub>, aerosols, or the ~~O<sub>2</sub>-O<sub>2</sub>~~ absorption which is commonly used to calculate the effective path length and the air mass factor [\(see Irizar et al. \(2019\)\)](#)

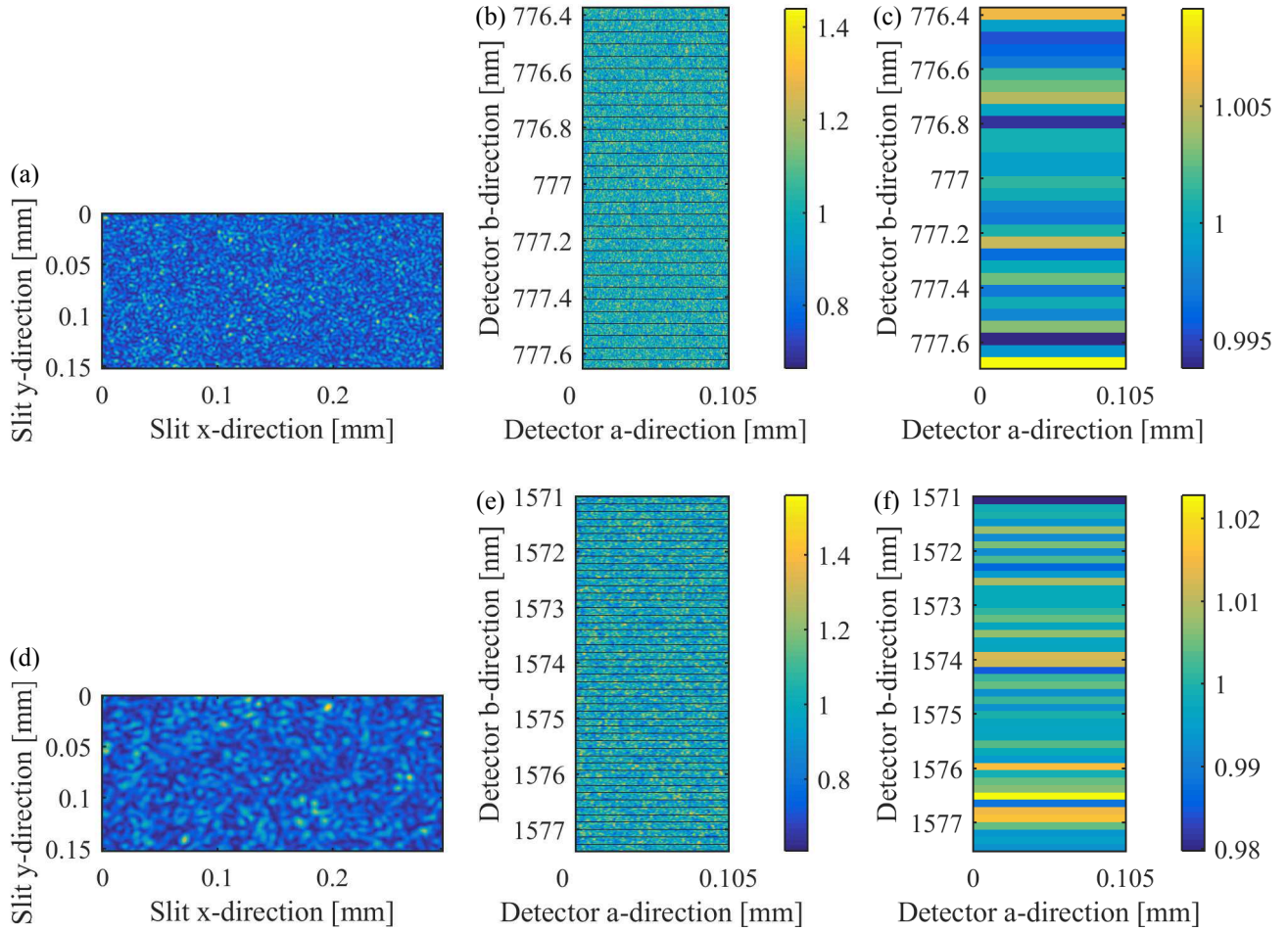


**Figure 2.**

Speckle patterns in the NIR band (a-c) and SWIR band (d-f) at different stages in the measurement chain: (a/d) is an example of a monochromatic speckle pattern in the slit plane, (b/e) is the speckle pattern integrated at the detector plane using Eq. (3) and normalized to its mean, where the horizontal lines denote the instrument detector pixel grid ( $\tilde{a}$ ,  $\tilde{b}$ ), and (c/f) is the final normalized integrated detector signal. The standard deviation taken over the pixel rows is the SFA.

, or Meijer et al. (2019), or Voors et al. (2017)). The experimental setup is shown in Sect. 3.1. As light sources serve tunable monochromatic external cavity diode lasers with single mode output and an integrated optical isolator. They are stabilized via a proportional-integral-derivative (PID) loop with feedback data from a wavemeter, which uses a Fizeau interferometer. As connecting fibers between laser, wavemeter, and output serve single mode (SM) fibers, since the spectral tuning range will be narrow. Also SM fiber will introduce no additional speckle in contrast to multi mode fibers. A linear polarizer ensures polarization stability. The round diffuser plate has a diameter of 70 mm and a thickness of 3 mm. It is made of highly

scattering fused silica HOD<sup>®</sup>-500 material ~~The~~ featuring inhomogeneities of 20 microns or less. The spatial coherence length of the Sun's light is around 60 microns in the NIR and 120 microns in the SWIR band, according to Divitt and Novotny (2015). Hence, the material, which was selected for the Sentinel-5/UVNS according to Irizar et al. (2019), is suited for the wavelengths in question and deemed a good choice for this study. The data collected with the powermeter is used to normalize the acquired images. The round apertures are used to control the size of individual speckle correlation areas. The laser beam's uniformity at the diffuser plane was measured to be around 3% in the NIR band and 6% in the SWIR band over the size of the aperture. There were no additional speckle contribution by the fibers detected. The telescope has a focal length of  $f_{tel} = 1100\text{mm}$ . For the NIR the laser source has a center wavelength of 780 nm and a nominal linewidth of ~~300~~  $6 \times 10^{-7}\text{nm}$ . The Thorlabs 780HP SM fiber type was used for all fiber connections in the NIR range. The CCD detector features a 12.5 mm x 10.0 mm active area with 2750 x 2200 pixels of size 4.54  $\mu\text{m}$  x 4.54  $\mu\text{m}$ . The expected speckle size average one dimensional width of the speckle correlation area  $S_d$  in the slit plane is calculated using

$$S_d = \frac{\lambda f_{tel}}{D/2\sqrt{\pi}} \frac{2\lambda f_{tel}}{D\sqrt{\pi}}, \quad (4)$$

where  $S_d$  is the width of the aperture function in the slit plane. ~~Thus a single speckle is sampled by 14~~ which was derived by Goodman (2007). The apertures' diameter is set to  $D = 10\text{mm}$ , and thus the speckles are sampled by 19 pixel in one dimension, which is deemed sufficiently fine to ensure that the sampling with the detector does not alter the speckle pattern significantly. The laser wavelength was tuned over the range of ~~776.0-776.4 nm-777.8-.7 nm~~ with a step size of  $\Delta\lambda = 1\text{pm}$ . The step size is chosen, so that there is a non zero correlation between subsequent speckle images. For the SWIR measurement the laser source as well as the detector and the fiber splitter are replaced and the Thorlabs SMF-28 SM fiber was used for fiber connections. The SWIR laser source center wavelength is 1550 nm, with single mode output of nominal ~~150 kHz~~  $2 \times 10^{-6}\text{nm}$  linewidth. The detector is a 640 x 512 pixel InGaAs camera with a pixel size of 15.5  $\mu\text{m}$  x 15.5  $\mu\text{m}$ . The tuning range was ~~1570nm-1573nm~~ 1571nm-1577.5nm with a step size of  ~~$\Delta\lambda = 2.5\text{pm}$~~   $\Delta\lambda = 3.1\text{pm}$ . The apertures' diameter is set to  ~~$D = 10\text{mm}$~~  yielding an estimated expected speckle oversampling ratio of 13.  ~~$D = 13\text{mm}$~~  which means a sampling of 10 pixel per speckle in one dimension. This is smaller than for the NIR configuration, but is a trade off between sampling and SNR.

#### 165 4 Spectral Features Amplitude Prediction Model

The prediction model presented in the following is a mathematical formulation of the measurement method described in Sect. 3. It relies on the determination of the speckle statistics at different steps of the measurement chain. The relevant physical information about speckle averaging effects in the measurement chain lies in the intensity distributions. A single pattern  $I$  is sampled by a finite but sufficient amount of pixel, so that the individual pixel size is small compared to the speckle size. The magnitude of the speckle effect in  $I$  is described as the *speckle contrast* (Goodman, 2007, p. 28)

$$C = \frac{\sigma_I}{\langle I \rangle}, \quad (5)$$

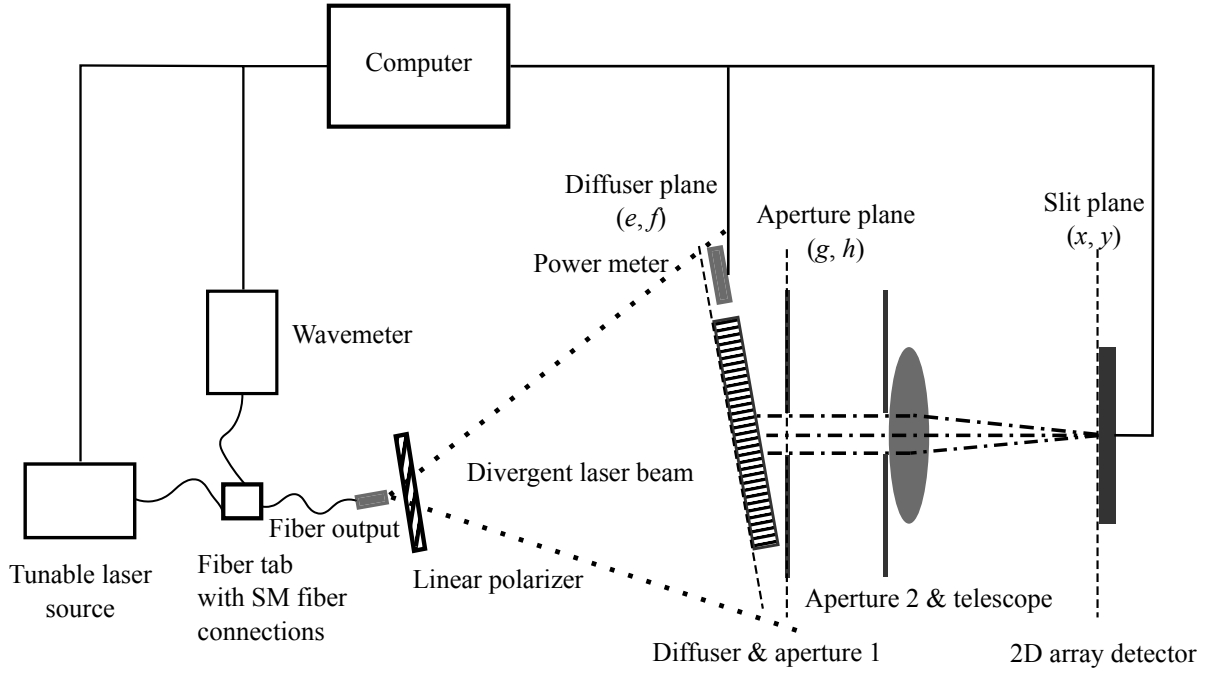


**Figure 3.**

Layout of the experimental setup for measuring diffuser induced monochromatic speckle patterns in the slit plane. [Single mode fibers indicated by curved lines are used to connect the laser source with the wavemeter and the output via a fiber tab.](#)

where  $\sigma_I$  is the standard deviation and  $\langle I \rangle$  is the mean value of  $I$  over all pixel. Under the general assumption, that the individual statistics of the underlying fields are circular complex Gaussian, a fully developed speckle pattern generated with linear polarized monochromatic light has a contrast of  $C = 1$  (Goodman, 2007, p. 29). We adopt this assumption for this model.

175 The speckle contrast is reduced by several averaging effects introduced by the spectrometer instrument. A reduction of  $C$  is only achieved by the summation of intensity distributions showing a correlation smaller than unity. If the summation is on amplitude basis (when the distributions can interfere),  $C$  is not reduced (Goodman, 2007, section 3.1.1). From this follows, that only distributions which can not interfere will impact  $C$  and are therefore subject of further discussions. Each one of the  $N$  independent averaging effects attributes to a certain amount of *degrees of freedom*  $M_n$  or effectively uncorrelated intensity  
180 distributions, which can be combined to a total averaging factor  $M$  ~~according to~~ (Goodman, 2007, p. 186) by

$$M = \prod_n^N M_n. \quad (6)$$

The reduced speckle contrast will then calculate to

$$C_{reduced} = \frac{1}{\sqrt{M}} = \left( \sqrt{\prod_n^N M_n} \right)^{-1}. \quad (7)$$

In order to predict the contrast reduction we identified  $N = 3$  contributors, which can be assigned to different steps of the SFA measurement chain:

1. Generation of monochromatic diffuse depolarized light in the aperture plane  $(g, h)$  yielding a factor  $M_{polarization}$ ,
2. mapping intensities in the slit plane  $(x, y)$  to instrument detector positions  $(a, b)$  contributing a factor  $M_{spectral}$ ,
3. and integration of the instrument detector pixels with a factor denoted by  $M_{detector}$ .

The predicted reduced speckle contrast at the instrument detector plane using Eq. (7) corresponds to the SFA and is

$$SFA = C_{reduced} = \frac{1}{\sqrt{M_{polarization} M_{spectral} M_{detector}}}. \quad (8)$$

#### 4.1 Polarization Averaging

The laser source emits a single polarization state, which is ensured with the polarizer. The diffuse light leaving the volume diffuser can be treated as depolarized due to multi scattering (Lorenzo, 2012, p.85). This corresponds to two orthogonal polarization configurations or two effective intensity distributions which can not interfere. Therefore step  $n = 1$  introduces two degrees of freedom  $M_{polarization} = 2$  (Goodman, 2007, p. 49).

#### 4.2 Spectral Averaging

Step  $n = 2$  leads to spectral averaging at the detector. We recall the finding from Sect. 3.1, that the net intensities in the field planes (slit and detector) can be treated as superposition of monochromatic intensities for integration times much greater than the coherence time. Let us consider the acquired speckle intensities  $I_n(x, y)$  and the underlying fields  $A_n(x, y)$ , which are related by  $I_n = |A_n|^2$ . They are recorded at frequencies  $f_n = \frac{c}{\lambda_n}$  with a difference  $\Delta f = f_m - f_n$  and  $c$  being the speed of light various wavelengths  $\lambda_n$ . The magnitude of the statistical change of subsequent speckle intensities  $I_m$  and  $I_n$  with a wavelength difference  $\Delta \lambda_{nm} = |\lambda_n - \lambda_m|$ , can be described in terms of the first order field correlation coefficient  $\mu_{mn}$ , with

$$\mu_{mn}(\Delta f) \left( \lambda_n, \lambda_m \right) = \frac{\langle A_m A_n^* \rangle}{\sqrt{\langle I_m \rangle \langle I_n \rangle}} \cdot \frac{\langle A_m A_n^* \rangle}{\sqrt{\langle I_m \rangle \langle I_n \rangle}}, \quad (9)$$

where  $*$  denotes the complex conjugate. The field correlation is influenced by two effects, which in our case are both frequency dependent. The first effect is due to changing light paths through the diffuser medium. The second effect takes into account the spatial offset  $\Delta b = k \frac{c}{\Delta f} \Delta \lambda_{nm}$  at the detector plane between individual speckle patterns  $I_n$  induced by the dispersion (see Eq. (2)). We start with the former contribution to the field correlation and follow the approach of Thompson et al. (1997a, b) and Webster et al. (2003), who used an analytic diffusion model to describe the light propagation in highly scattering, non-absorbing diffusers. The diffusion model yields the path length probability density function  $p(l)$  depending on the properties of the diffuser material, namely the scattering Zhu et al. (1991), who presented an analytic equation

for the angular correlation function of a slab geometry of a scattering media of thickness  $d$ , which can also be used for wavelength correlations:

$$F(\lambda_n, \lambda_m) = \frac{(d + 2B)/(z_0 + B) \left[ \sinh(z_0 \sqrt{q^2 + \alpha^2}) + B \sqrt{q^2 + \alpha^2} \cosh(z_0 \sqrt{q^2 + \alpha^2}) \right]}{[1 + B^2(q^2 + \alpha^2)] \sinh(d \sqrt{q^2 + \alpha^2}) + 2B \sqrt{q^2 + \alpha^2} \cosh(d \sqrt{q^2 + \alpha^2})}, \quad (10)$$

215 where we set  $q = \sqrt{i6\pi \left| \frac{1}{\lambda_n} - \frac{1}{\lambda_m} \right| \beta n_s / l_t}$ , with  $n_s$  denoting the refractive index of the scattering material,  $l_t$  the transport mean free path length  $l_s$ , the refractive index of the material  $n_s$ , and the thickness  $d$ . The characteristic function  $F_l(\Delta f)$  is the frequency-dependent representation of  $p_l(t)$  and is given by

$$F_l(\Delta f) = \int_0^\infty p_l(t) \exp\left(\frac{i2\pi(1 - n_s)\Delta f \alpha l}{c}\right) dt,$$

220 where  $e$  denotes the speed of light and  $\alpha$  used for anisotropic multi scattering systems, and  $\beta$  a constant factor taking into account the contribution of the tilted diffuser plane ( $e, f$ ) with respect to the other planes and the specific geometry. The value  $z_0$  describes the average penetration depth after which the light is scattered for the first time. It does not have a great influences in a transmission geometry and is approximated with the transport mean free path  $l_t$ . We set  $\alpha = 0$ , thereby ignoring absorption. The parameter for the boundary condition is given by  $B = l_t \frac{2(1+R)}{3(1-R)}$ , where  $R$  is the reflection coefficient which is calculated using the Fresnel equations. It accounts for internal reflection due to index of refraction mismatch at the boundaries.

225 The second contribution to the field correlation is due to changing spatial positions of speckle patterns which are distributed over the instrument detector in accordance with the spectral dispersion. This constitutes a spatial offset  $\Delta b(\Delta f)$  between the speckle intensities  $I_n$  and  $I_m$  at the detector plane ( $a, b$ ). Keeping in mind Eq. (1) and (2) for the transformation from the slit to the detector plane, the correlation of speckle fields, which are separated spatially by  $\Delta b$  can be expressed as

$$\Psi(\Delta a, \Delta b) \Big|_{\Delta a=0} = \frac{\int_{-\infty}^{\infty} |P(h)|^2 e^{-i\frac{2\pi}{\lambda z} h \Delta b} dh}{\int_{-\infty}^{\infty} |P(h)|^2 dh} \frac{\int_{-\infty}^{\infty} |P(g, h)|^2 e^{-i\frac{2\pi}{\lambda z} (g \Delta a + h \Delta b)} dg dh}{\int_{-\infty}^{\infty} |P(g, h)|^2 dg dh} \Big|_{\Delta a=0}, \quad (11)$$

230 where  $P(h)$   $P(g, h)$  is the aperture function of the imaging system,  $h$  is the  $y$  and may be defined, e.g. for a circular aperture of diameter  $D$ , as  $P(g, h) = \text{circ}\left(\frac{2\sqrt{g^2 + h^2}}{D}\right)$  which is 1 inside the aperture and 0 otherwise,  $g$  and  $h$  are the  $a$ - and  $b$ -coordinate representations in the aperture plane,  $z$  is the distance between pupil and image aperture and slit plane, and  $\lambda$  the mean wavelength (Goodman, 2007, p. 169). We set  $\Delta a = 0$  since we are only interested in the offset in the spectral direction. Combining the two frequency-dependent effects we can model the correlation between the speckle fields as

$$235 \mu_{mn}(\Delta f) \left( \lambda_n, \lambda_m \right) = F_l(\Delta f) \left( \lambda_n, \lambda_m \right) \Psi(\Delta b(\Delta f)). \quad (12)$$

The accumulation of individual speckle patterns  $I_n$  with field correlations  $\mu_{mn}$  at the detector can be interpreted as the summation of partially correlated speckle intensities

$$I_{det}(a, b) = \sum_{n=1}^{N=\lambda_{res}/\Delta\lambda} I_n \left( \frac{a}{M_x}, \frac{b - k\lambda}{M_y}, \frac{c}{\lambda_n} \right). \quad (13)$$

The amount of individual speckle intensities  $I_n$  contributing to the sum at arbitrary detector coordinates  $(a, b)$  is equal to the ratio of the spectral resolution  $\lambda_{res}$  with the step size  $\Delta\lambda$ . This also applies to the mean intensities,

$$\langle I_{det}(a, b) \rangle = \sum_{n=1}^{N=\lambda_{res}/\Delta\lambda} \langle I_n \left( \frac{a}{M_x}, \frac{b - k\lambda}{M_y}, \frac{c}{\lambda_n} \lambda_n \right) \rangle. \quad (14)$$

Using an established method shown by Bevan (2009) and Goodman (2007) we define a coherency matrix with entries  $J_{nm} = \langle A_m A_n^* \rangle$  and use Eq. (9) to get

$$\underline{\underline{J}} = \begin{bmatrix} \langle I_1 \rangle & \sqrt{\langle I_1 \rangle \langle I_2 \rangle} \mu_{1,2} & \cdots & \sqrt{\langle I_1 \rangle \langle I_N \rangle} \mu_{1,N} \\ \sqrt{\langle I_1 \rangle \langle I_2 \rangle} \mu_{1,2}^* & \langle I_2 \rangle & \cdots & \sqrt{\langle I_2 \rangle \langle I_N \rangle} \mu_{2,N} \\ \vdots & \vdots & \ddots & \vdots \\ \sqrt{\langle I_1 \rangle \langle I_N \rangle} \mu_{1,N}^* & \sqrt{\langle I_2 \rangle \langle I_N \rangle} \mu_{2,N}^* & \cdots & \langle I_N \rangle \end{bmatrix}. \quad (15)$$

By diagonalization of  $\underline{\underline{J}}$  with a unitary linear transformation  $\underline{\underline{L}}_0 \underline{\underline{L}}_0^\dagger$ , the ensemble of correlated speckle fields is transformed to a basis with no correlation between them.

$$\underline{\underline{J}}' = \underline{\underline{L}}_0 \underline{\underline{J}} \underline{\underline{L}}_0^\dagger = \begin{bmatrix} \langle \tilde{I}_1 \rangle & 0 & \cdots & 0 \\ 0 & \langle \tilde{I}_2 \rangle & \cdots & 0 \\ \vdots & \vdots & \ddots & \vdots \\ 0 & 0 & \cdots & \langle \tilde{I}_N \rangle \end{bmatrix}, \quad (16)$$

where  $\dagger$  denotes the Hermitian transpose operation. The total mean intensity  $\langle I_{det} \rangle = \sum_n \langle I_n \rangle = \sum_n \langle \tilde{I}_n \rangle$  is conserved under this transformation but in general  $\langle I_n \rangle \neq \langle \tilde{I}_n \rangle$ . The complex coherence factor  $\mu_{mn} = |\mu_{mn}| \exp(i\Phi_{nm})$  includes a phase  $\Phi_{nm}$ . However, due to the specific construction of  $\underline{\underline{J}}$ , these phase terms can be omitted when calculating the eigenvalues (Dainty et al., 1975, section 4.7.2). Finally, for the spectral degrees of freedom we use the eigenvalues  $\langle \tilde{I}_n \rangle$  of the coherency matrix to get

$$M_{spectral} = \left( \frac{\langle I_{det} \rangle}{\sigma_{det}} \right)^2 = \frac{\left( \sum_n \langle \tilde{I}_n \rangle \right)^2}{\sum_n \langle \tilde{I}_n \rangle^2}. \quad (17)$$

Note that changing  $\Delta\lambda$  to a smaller step size and therefore increasing and thus changing  $N$  will not change the result of  $M_{spectral}$  as long as  $\Delta\lambda$  is sufficiently small to sample the covariance  $\mu_{mn}$ . The enabling property of the coherency matrix  $\underline{\underline{J}}$  is called *Toeplitz*, which implies an asymptotically behavior of its eigenvalues found by Grenander and Szegö (1958). Gray (2006) gives a simplified prove in Corollary 2.1 and 2.2 that both, numerator and denominator in Eq. (17) converge for large  $N$ .

### 4.3 Detector Averaging

In step  $n = 3$  an averaging due to the integration of the instrument detector pixel takes place. We already established, that the resultant intensity distribution at the detector  $I_{det}(a, b)$  is given by the summation in Eq. (13). This effect impacts the speckle

contrast if individual speckles are not sufficiently oversampled by the instrument detector pixel grid  $(\tilde{a}, \tilde{b})$ . An analytical expression for the degrees of freedom  $M_{detector}$  introduced by stationary speckles in one detector pixel with relative coordinates  $(\Delta a, \Delta b)$  is given by

$$265 \quad M_{detector} = \left[ \frac{1}{A_D^2} \iint_{-\infty}^{\infty} K_D(\Delta a, \Delta b) |\mu_{det}(\Delta a, \Delta b)|^2 d\Delta a d\Delta b \right]^{-1}, \quad (18)$$

where  $A_D$  is the area of a detector pixel,  $K_D(\Delta a, \Delta b)$  is the autocorrelation function of the detector pixel, and  $\mu_{det}(\Delta a, \Delta b)$  is the field correlation at the detector plane (Goodman, 2007, p. 108). In order to accurately describe  $\mu_{det}$  one needs to account for the evolution of the speckle size during the summation in Eq. (13). Let us consider a single speckle correlation area  $I_1(S_d/2 \leq |x_1|, S_d/2 \leq |y_1|, f_1)$   $I_1(S_d/2 \leq |x - x_1|, S_d/2 \leq |y - y_1|, \lambda_1)$  with a spatial extend denoted by  $S_d$  centered at  $(x_1, y_1)$  in the slit. Its correlation relative to this position is described by

$$270 \quad \Psi(\Delta x, \Delta y) = \frac{\int_{-\infty}^{\infty} |P(g, h)|^2 e^{-i \frac{2\pi}{\lambda_x} (g\Delta x + h\Delta y)} dg dh}{\int_{-\infty}^{\infty} |P(g, h)|^2 dg dh} \frac{\int_{-\infty}^{\infty} |P(g, h)|^2 e^{-i \frac{2\pi}{\lambda_x} (g\Delta x + h\Delta y)} dg dh}{\int_{-\infty}^{\infty} |P(g, h)|^2 dg dh}, \quad (19)$$

with  $\Delta x = x - x_1$  and  $\Delta y = y - y_1$  being relative coordinates. The function  $F_1(\Delta f)$   $F(\lambda_1, \lambda_n)$  introduced previously, characterizes how the correlation area develops after  $n$  frequency-wavelength steps at the same position,  $I_n(S_d/2 \leq |x_1|, S_d/2 \leq |y_1|, f_n)$   $I_n(S_d/2 \leq |\Delta x|, S_d/2 \leq |\Delta y|, \lambda_n)$  with  $n > 1$ . In other words, it denotes the amount of spectral steps after which a single speckle ceases to exist at a fixed position in the slit. The initial position of the speckle at the detector is  $(a_1, b_1) = (M_x x_1, M_y y_1 + k \frac{c}{f_1})(a_1, b_1)$ . The subsequent contributions relative to the initial position are shifted by  $k(\frac{c}{f_1} - \frac{c}{f_n})$  in the  $b$ -direction by  $k|\lambda_1 - \lambda_n|$  and have a magnitude denoted by  $F_1(f_1 - f_n)$   $F(\lambda_1, \lambda_n)$ . Therefore, the resultant speckle correlation function at the detector  $\mu_{det}(\Delta a, \Delta b)$   $|\mu_{det}(\Delta a, \Delta b)|^2$  is a convolution of  $|\Psi(\Delta a, \Delta b(\Delta f))|^2$  with  $|F_1(\Delta f)|^2$ .

#### 4.4 Predicted SFA

280 The predicted reduced speckle contrast at the instrument detector plane using Eq. (7) corresponds to the SFA and is

$$SFA = C_{reduced} = \frac{1}{\sqrt{M_{polarization} M_{spectral} M_{detector}}}.$$

$|\Psi(\Delta a, \Delta b)|^2$  with  $|F(\lambda_n, \lambda_m)|^2$ :

$$|\mu_{det}(\Delta a, \Delta b)|^2 = |\Psi(\Delta a, \Delta b)|^2 \otimes |F(\lambda_n, \lambda_m)|^2. \quad (20)$$

The symbol  $\otimes$  denotes the convolution.

## 285 5 Results and Discussion

In the following we present and compare the SFA results from the measurement chain of Sect. 3 with the ones from the prediction model of Sect. 4 in the NIR and SWIR regime.  $M_{spectral}$  can be interpreted as the average number of speckle

patterns generated by the diffuser per spectral channel at the given wavelengths.  $M_{detector}$  can be understood as average number of speckle correlation areas influencing the measurement in a detector pixel. The values of relevant parameters used are depicted in Table 1. They were chosen to represent a proposed instrument for ESA's CO2M mission (Meijer et al. (2019)). In Figure 4 the measured Pearson correlations between speckle patterns  $I_n(\lambda_n)$  and  $I_m(\lambda_m)$  with respect to their relative spectral distance is shown as blue stars for the NIR band at 776 nm and the SWIR band at 1571 nm, respectively. All wavelength shift combinations up to 0.1 nm are averaged for 120 images. Error bars are omitted, because the standard error of the mean is too small to be displayed. The red line denotes a fit to Eq. (10) leading to the values for  $l_t$  depicted in Table 1. They are in agreement with the supplier's given value of  $l_t = 56 \mu\text{m}$  at 500 nm wavelength.

**Table 1.** Sample spectrometer parameters used for the measurement and prediction. They were chosen to represent a proposed instrument for ESA's CO2M mission (Meijer et al. (2019)).

parameter-Parameter	Value
Magnification $M_x$	0.34
Magnification $M_y$	0.30
aperture-Aperture diameter	40.0 mm
slit-Slit dimensions (x, y-direction)	295 $\mu\text{m}$ , 152 $\mu\text{m}$
detector-Detector dimensions (a, b-direction)	105 $\mu\text{m}$ , 45 $\mu\text{m}$
telescope-Telescope focal length	131 mm
Diffuser thickness $d$	3 mm
<del><math>l_s = 53 \mu\text{m}</math></del>	
NIR specific	
Spectral resolution $\lambda_{res}$	<del>0.12</del> 0.128 nm
Spectral tuning range $\lambda_1 \dots \lambda_N$	<del>776.0-776.4</del> nm - <del>777.8-777.7</del> nm
<del><math>n_s = 1.454</math></del> Tuning step size $\Delta\lambda$	1 pm
Refractive index of diffuser material $n_s(\lambda)$	1.454
Mean free path $l_t(\lambda)$	(59.3 $\pm$ 0.4) $\mu\text{m}$
SWIR specific	
Spectral resolution $\lambda_{res}$	0.4 nm
Spectral tuning range $\lambda_1 \dots \lambda_N$	1571 nm - <del>1573.5-1577.5</del> nm
<del><math>n_s = 1.444</math></del> Tuning step size $\Delta\lambda$	<del>2.5-3.1</del> pm
Refractive index of diffuser material $n_s(\lambda)$	1.444
Mean free path $l_t(\lambda)$	(67.8 $\pm$ 0.5) $\mu\text{m}$

By calculating the frequency correlation of subsequent monochromatic speckle images  $I(x, y, \frac{c}{f_n})$  the fitted mean free path length of our diffuser sample is determined as  $l_s = 53 \mu\text{m}$ , which is close to the manufactures' specification of 55  $\mu\text{m}$ . This

value may also reflect small instabilities of the speckle stationarity in the slit plane, which induce a smaller correlation between subsequent speckle intensities and therefore a shorter effective mean free path length.

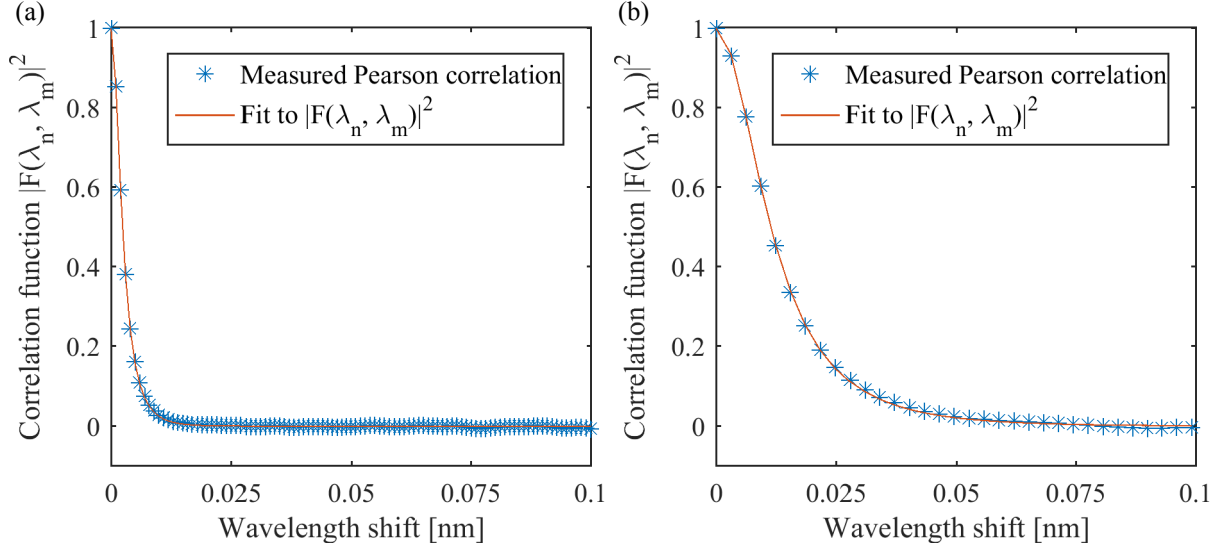


**Figure 4.** Measurement of the correlation function  $|F(\lambda_n, \lambda_m)|$  in (a) the NIR (776 nm) and (b) the SWIR band (1571 nm). Blue stars denote the measured Pearson correlations between speckle patterns  $I_n(\lambda_n)$  and  $I_m(\lambda_m)$ . All wavelength shift combinations up to 0.1 nm are averaged for 120 images. Error bars are omitted, because the standard error of the mean value is too small to be displayed. The red graph denotes the fit of the measured data points to Eq. (10) with (a)  $l_t = (59.3 \pm 0.4) \mu\text{m}$  and (b)  $l_t = (67.8 \pm 0.5) \mu\text{m}$ .

300 Table 2 shows the SFA values of the measurements and predictions with their corresponding intermediate averaging factors  $M_{polarization}$ ,  $M_{spectral}$ , and  $M_{detector}$  introduced in Sect. 4. Their counterparts from the measurement are deduced by calculating the speckle contrast at intermediate steps in the measurement chain. To verify the factor  $M_{polarization} = 2$  a linear polarizer is placed *after* the diffuser and the measured speckle contrast compared to the nominal case rises by a factor of  $\sqrt{2}$ . Additionally, the polarization axis is rotated to different random positions without changing the result, which confirms the  
305 assumption made in Sect. 4, that the light exiting the diffuser is depolarized. With an ideal measurement chain the speckle contrast expected in the slit plane for monochromatic polarized speckles is  $C_{slit,ideal} = 1$ . This is the numerator in Eq. (8). The measured contrast in the slit is smaller, probably due to detector noise as suggested by Postnov et al. (2019). Webster et al. (2003) attributed the reduced measured contrast straylight from multiple reflections in their setup. The experimental factors  $M_{spectral,measured}$  and  $M_{detector,measured}$  are calculated in similar way using the relations,

$$310 \quad C_{spectral,measured} = \frac{\langle C_{slit,measured} \rangle}{\sqrt{M_{spectral,measured}}}, \quad (21)$$

$$C_{detector,measured} = \frac{\langle C_{spectral,measured} \rangle}{\sqrt{M_{detector,measured}}} \frac{C_{spectral,measured}}{\sqrt{M_{detector,measured}}}. \quad (22)$$

Type	$M_{polarization}$	$M_{spectral}$	$M_{detector}$	$SFA_{SFA}$ [%]
Measurement NIR	2	$59.55.9 \pm 0.7$	$548 (6.1 \pm 1.8) \times 10^2$	$0.00400.38 \pm 0.06$
Prediction NIR	2	$55.56.5$	$536.5.7 \times 10^2$	$0.00410.39$
Measurement SWIR	2	$31.29.9 \pm 0.8$	$192 (1.7 \pm 0.4) \times 10^2$	$0.00920.99 \pm 0.12$
Prediction SWIR	2	$30.30.0$	$191.1.8 \times 10^2$	$0.00930.96$

**Table 2.** Comparison SFA results of the measurement chain with the prediction model. Measurement uncertainties are given in the  $1\sigma$  interval.

The results show a good agreement of prediction model and measurement. ~~For the NIR regime the measured spectral averaging~~  
 ~~$M_{spectral}$  is 7~~ and are well within the estimated error margins, which are given in the  $1\sigma$  interval. While the spectral extent of  
a speckle correlation area at the detector can be derived from the width of  $\mu_{det}$ , one can also see from the values of  $M_{detector}$ ,  
315 ~~that the extent must be small compared to a pixel. This allows for the treatment of the SFA as white noise on detector level,~~  
~~which can be a goal of the instrument design. The uncertainties  $\Delta M_{spectral,measured}$  and  $\Delta M_{detector,measured}$  are estimated~~  
~~by considering fluctuations in the two contributors  $F$  and  $\Psi$  to the field correlation  $\mu_{mn}$  in Eq. (12) and  $\mu_{det}$  in Eq. (20).~~  
~~For  $F$  the measured standard deviation of each data point in Figure 4 is taken as a measure, which amounts to 1-2 % higher,~~  
~~than predicted. We assume, that detector noise is averaged in this step, which will yield a higher effective averaging factor.~~  
320 ~~The SWIR measurement spectral averaging factor shows a smaller deviation of 2, which we also attribute to averaged detector~~  
~~noise. The measured detector averaging factor in the NIR and 2-3 % in the SWIR band. The average fluctuations of  $\Psi$  were~~  
~~determined by measuring its width over 120 speckle patterns by autocorrelation to be 1.3 % and 2.7 % in the NIR and SWIR,~~  
~~respectively. The impact on the  $M_{spectral,measured}$  and  $M_{detector,measured}$  is estimated by a Monte Carlo propagation of~~  
~~both uncertainties. It yields that those two factors are the major contributors to the uncertainty  $\Delta M_{spectral}$ . This approach~~  
325 ~~also accounts for detector noise, if it caused the fluctuations. The impact on  $M_{detector}$  for both wavelength regimes indicates~~  
~~no correlation of features between adjacent instrument detector pixel due to its high value (Goodman, 2007, p. 109). It is~~  
~~also dependent on detector noise, which explains the slightly higher averaging factors than predicted-, however, is small. It~~  
~~was deduced from Ahn and Fessler (2003), that  $\Delta M_{detector}$  is primarily caused by the uncertainty of the standard deviation~~  
~~estimator for a small amount of samples. In our case the sample number equals the amount of detector pixel (see Figure 2),~~  
330 ~~which is  $n = 30$  for the NIR and  $n = 48$  for the SWIR measurement. The uncertainties presented also reflect the fact that the~~  
~~SFA is not constant over a wavelength range of a few nanometers as illustrated in Figure 5. It shows plots of the SFA scaling~~  
~~with wavelength for a CO2I like instrument in the NIR and SWIR band calculated with the prediction model. The linear~~  
~~dependency only holds under the assumption of a constant dispersion, which is usually not the case for a realistic instrument.~~  
~~However, this result gives a clear indication to the general scaling of the speckle effect.~~

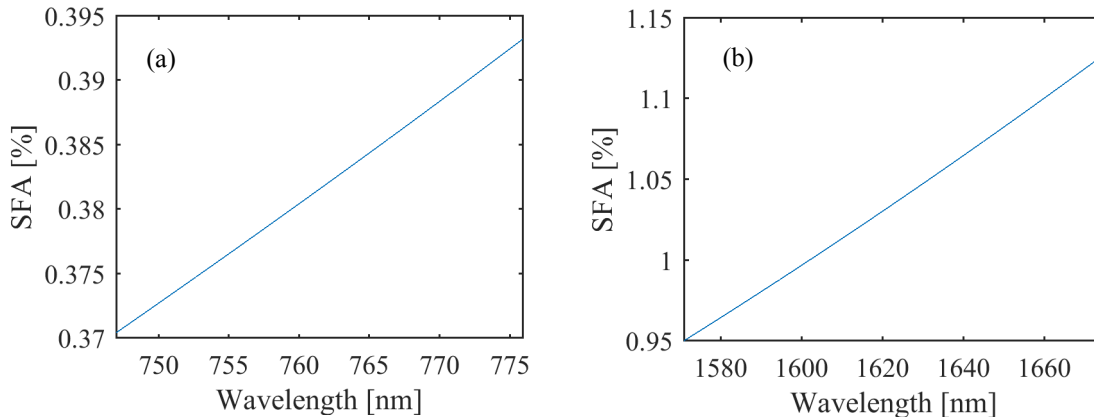


Figure 5. Scaling of the SFA with wavelength of a CO2I like instrument in the (a) NIR and (b) SWIR band using the prediction model.

## 335 6 Conclusions

We demonstrated a comprehensive and numerical approach to quantify diffuser induced spectral features during solar calibration of space imaging spectrometers, which is based on established speckle theory concepts. We compared our prediction results with our current measuring method and observed a good agreement. We also give an indication regarding the wavelength dependency of the effect. The presented speckle averaging mechanisms are not a complete representation of the real in-orbit situation of an instrument. The effect of the Sun’s disk, which consists of many incoherent points sources distributed over a 0.5 degree angle, needs to be taken into account as well as the averaging due to the movement of the instrument relative to the Sun. Also, unlike the used laser point sources for the measurements, the Sun’s light features an additional orthogonal polarization state, adding two polarization configurations to  $M_{polarization}$  in the case of a highly scattering volume diffuser. The presented approach can be used for other diffuser types and optical geometries as well. It provides a solid starting point for future investigations into angular averaging mechanisms, which will complement the description of speckle reduction effects in imaging spectrometers of this type.

*Data availability.* The datasets generated and/or analyzed for this work are available from the corresponding author on reasonable request, subject to confirmation of Airbus Defence and Space GmbH.

*Author contributions.* Florian Richter was responsible for the acquisition and the analysis of the measurement data supported by all co-authors. Florian Richter developed the prediction model supported by Jerome Caron with insights about polarization contributions, spectral

averaging, and properties of coherency matrices and revised by Corneli Keim and Mark Wenig. Florian Richter prepared the manuscript with contributions and critical revision from all co-authors.

*Competing interests.* The authors declare, that they have no conflict of interest.

*Acknowledgements.* The fused silica diffuser HOD<sup>®</sup>-500 used in this work was provided by Frank Nürnberg and Bernhard Franz, Heraeus  
355 Conamic, Germany.

## References

- Agarwal, G. S., Gbur, G., and Wolf, E.: Coherence properties of sunlight, *Opt. Lett.*, 29, 459–461, <https://doi.org/10.1364/OL.29.000459>, <http://ol.osa.org/abstract.cfm?URI=ol-29-5-459>, 2004.
- Ahlers, B., Courreges-Lacoste, G. B., Schrijvers, C., and van Brug, H.: In-orbit detection of spectral features in SCIAMACHY, in: *Sensors, Systems, and Next-Generation Satellites VIII*, edited by Meynart, R., Neeck, S. P., and Shimoda, H., SPIE, <https://doi.org/10.1117/12.565565>, 2004.
- Ahn, S. and Fessler, J.: *Standard Errors of Mean, Variance, and Standard Deviation Estimators*, 2003.
- Bevan, A.: *Statistical Data Analysis for the Physical Sciences*, Cambridge University Press, <https://doi.org/10.1017/cbo9781139342810>, 2009.
- 365 Bianco, V., Memmolo, P., Leo, M., Montresor, S., Distante, C., Paturzo, M., Picart, P., Javidi, B., and Ferraro, P.: Strategies for reducing speckle noise in digital holography, *Light: Science and Applications*, 7, 48, <https://doi.org/10.1038/s41377-018-0050-9>, 2018.
- Burns, T., Ferreria, L., Keim, C., Prieto, L. P., Krauser, J. S., and Weise, D.: Sentinel-5: a novel measurement approach to quantify diffuser induced spectral features, in: *International Conference on Space Optics — ICSO 2016*, edited by Karafolas, N., Cugny, B., and Sodnik, Z., SPIE, <https://doi.org/10.1117/12.2296079>, 2017.
- 370 Clermont, L., Mazy, E., Marquet, B., and Plessier, J.-Y.: An in-flight calibration assembly for the earth observation instrument Sentinel-4 UVN, in: *Astronomical Optics: Design, Manufacture, and Test of Space and Ground Systems II*, edited by Hallibert, P., Hull, T. B., and Kim, D. W., SPIE, <https://doi.org/10.1117/12.2529572>, 2019.
- Dainty, J. C., Ennos, A. E., Françon, M., Goodman, J. W., McKechnie, T. S., and Parry, G.: *Laser Speckle and Related Phenomena*, Springer Berlin Heidelberg, <https://doi.org/10.1007/bfb0111434>, 1975.
- 375 Divitt, S. and Novotny, L.: Spatial coherence of sunlight and its implications for light management in photovoltaics, *Optica*, 2, 95–103, <https://doi.org/10.1364/OPTICA.2.000095>, <http://www.osapublishing.org/optica/abstract.cfm?URI=optica-2-2-95>, 2015.
- Fletcher, K., Rider, H., and Agency, E. S.: *Report for Mission Selection: Carbonsat Flex*, ESA SP, ESA Communication Production Office, <https://books.google.de/books?id=nkyrDAEACAAJ>, 2015.
- Goodman, J. W.: *Speckle Phenomena in Optics: Theory and Application*, Roberts & Company Publishers, 2007.
- 380 Gray, R. M.: *Toeplitz and Circulant Matrices: A review*, 2006.
- Grenander, U. and Szegő, G.: *Toeplitz Forms and their Applications*, University of California Press, 1958.
- Guehne, T., Keim, C., Bartsch, P., Weiss, S., Melf, M., and Seefelder, W.: Sentinel-5 instrument: status of design, performance, and development, in: *Sensors, Systems, and Next-Generation Satellites XXI*, SPIE, <https://doi.org/10.1117/12.2278564>, 2017.
- Hecht, E. and Lippert, K.: *Optik*, De Gruyter, Berlin, Boston, <https://doi.org/https://doi.org/10.1515/9783110526653>, <https://www.degruyter.com/view/title/525251>, 2018.
- 385 Heeman, W., Steenbergen, W., van Dam, G. M., and Boerma, E. C.: Clinical applications of laser speckle contrast imaging: a review, *Journal of Biomedical Optics*, 24, 1 – 11, <https://doi.org/10.1117/1.JBO.24.8.080901>, <https://doi.org/10.1117/1.JBO.24.8.080901>, 2019.
- Irizar, J., Melf, M., Bartsch, P., Koehler, J., Weiss, S., Greinacher, R., Erdmann, M., Kirschner, V., Albinana, A. P., and Martin, D.: Sentinel-5/UVNS, in: *International Conference on Space Optics 2018*, edited by Sodnik, Z., Karafolas, N., and Cugny, B., vol. 11180, pp. 41 – 58, International Society for Optics and Photonics, SPIE, <https://doi.org/10.1117/12.2535923>, <https://doi.org/10.1117/12.2535923>, 2019.
- 390 Lorenzo, J. R.: *Principles of Diffuse Light Propagation*, World Scientific Publishing Company, [https://www.ebook.de/de/product/11434141/jorge\\_ripoll\\_lorenzo\\_principles\\_of\\_diffuse\\_light\\_propagation.html](https://www.ebook.de/de/product/11434141/jorge_ripoll_lorenzo_principles_of_diffuse_light_propagation.html), 2012.

- Martimort, P., Fernandez, V., Kirschner, V., Isola, C., and Meygret, A.: Sentinel-2 MultiSpectral imager (MSI) and calibration/validation, in: 2012 IEEE International Geoscience and Remote Sensing Symposium, IEEE, <https://doi.org/10.1109/igarss.2012.6351960>, 2012.
- 395 Meijer, Y., Boesch, H., Bombelli, A., Brunner, D., Buchwitz, M., Ciais, P., Crisp, D., Engelen, R., Holmlund, K., Houweling, S., Janssens-  
Meanhout, G., Marshall, J., Nakajima, M., B.Pinty, Scholze, M., Bezy, J.-L., Drinkwater, M., Fehr, T., Fernandez, V., Loescher, A.,  
Nett, H., and Sierk, B.: Copernicus CO2 Monitoring Mission Requirements Document, techreport 2, European Space Agency, Earth and  
Mission Science Division, 2019.
- Nieke, J. and Mavrocordatos, C.: Sentinel-3a: commissioning phase results of its optical payload, in: International Conference on Space  
400 Optics — ICSO 2016, edited by Karafolas, N., Cugny, B., and Sodnik, Z., SPIE, <https://doi.org/10.1117/12.2296174>, 2017.
- Olij, C., Schaarsberg, J. G., Werij, H. G., Zoutman, E., Baudin, G., Chommeloux, B., Bezy, J.-L., and Gourmelon, G.: Spectralon diffuser cali-  
bration for MERIS, in: Sensors, Systems, and Next-Generation Satellites, edited by Fujisada, H., SPIE, <https://doi.org/10.1117/12.298122>,  
1997.
- Postnov, D. D., Cheng, X., Erdener, S. E., and Boas, D. A.: Choosing a laser for laser speckle contrast imaging, Scientific Reports, 9,  
405 <https://doi.org/10.1038/s41598-019-39137-x>, 2019.
- Richter, A., Wittrock, F., Ladstaetter-Weissenmayer, A., and Burrows, J.: Gome measurements of stratospheric and tropospheric BrO, Ad-  
vances in Space Research, 29, 1667–1672, [https://doi.org/10.1016/s0273-1177\(02\)00123-0](https://doi.org/10.1016/s0273-1177(02)00123-0), 2002.
- Richter, F., Krauser, J. S., Keim, C., Weise, D., and Wenig, M.: A novel measurement approach to quantify diffuser induced Spectral  
Features, in: Sensors, Systems, and Next-Generation Satellites XXII, edited by Neeck, S. P., Kimura, T., and Martimort, P., SPIE,  
410 <https://doi.org/10.1117/12.2501943>, 2018.
- Thompson, C. A., Webb, K. J., and Weiner, A. M.: Imaging in scattering media by use of laser speckle, Journal of the Optical Society of  
America A, 14, 2269, <https://doi.org/10.1364/josaa.14.002269>, 1997a.
- Thompson, C. A., Webb, K. J., and Weiner, A. M.: Diffusive media characterization with laser speckle, Applied Optics, 36, 3726,  
<https://doi.org/10.1364/ao.36.003726>, 1997b.
- 415 van Brug, H. and Courrèges-Lacoste, G. B.: Spectral features, effects, and cures, in: Earth Observing Systems XII, edited by Butler, J. J. and  
Xiong, J., SPIE, <https://doi.org/10.1117/12.731012>, 2007.
- van Brug, H. and Scalia, P. S.: New approach to spectral features modeling, in: Earth Observing Systems XVII, edited by Butler, J. J., Xiong,  
X., and Gu, X., SPIE, <https://doi.org/10.1117/12.931497>, 2012.
- van Brug, H. H., Vink, R., Schaarsberg, J. G., Courreges-Lacoste, G. B., and Snijders, B.: Speckles and their effects in spectrometers due to  
420 on-board diffusers, in: Earth Observing Systems IX, edited by Barnes, W. L. and Butler, J. J., SPIE, <https://doi.org/10.1117/12.559596>,  
2004.
- Voors, R., de Vries, J., Bhatti, I. S., Lobb, D., Wood, T., van der Valk, N., Aben, I., and Veefkind, P.: TROPOMI, the Sentinel 5 precursor  
instrument for air quality and climate observations: status of the current design, in: International Conference on Space Optics 2012,  
edited by Cugny, B., Armandillo, E., and Karafolas, N., vol. 10564, pp. 442 – 446, International Society for Optics and Photonics, SPIE,  
425 <https://doi.org/10.1117/12.2309017>, <https://doi.org/10.1117/12.2309017>, 2017.
- Webster, M. A., Webb, K. J., Weiner, A. M., Xu, J., and Cao, H.: Temporal response of a random medium from speckle intensity frequency  
correlations, Journal of the Optical Society of America A, 20, 2057, <https://doi.org/10.1364/josaa.20.002057>, 2003.
- Wenig, M., Kuehl, S., Beirle, S., Bucsele, E., Jaehne, B., Platt, U., Gleason, J., and Wagner, T.: Retrieval and analysis of strato-  
spheric NO2 from the Global Ozone Monitoring Experiment, Journal of Geophysical Research: Atmospheres, 109, n/a–n/a,  
430 <https://doi.org/10.1029/2003jd003652>, 2004.

Zhu, J. X., Pine, D. J., and Weitz, D. A.: Internal reflection of diffusive light in random media, *Phys. Rev. A*, 44, 3948–3959, <https://doi.org/10.1103/PhysRevA.44.3948>, <https://link.aps.org/doi/10.1103/PhysRevA.44.3948>, 1991.